Experimental Study of the Stability of the Bödewadt Layer

R. J. Lingwood[1] and P. H. Alfredsson[2]

[1] Department of Engineering, University of Cambridge, Trumpington Street, Cambridge CB2 1PZ, UK
[2] Department of Mechanics, Royal Institute of Technology, S–100 44, Stockholm, Sweden

Abstract. This work is concerned with the establishment and stability of the Bödewadt layer. A close approximation to the Bödewadt similarity solution can be achieved experimentally on the stator of an enclosed rotor-stator system. The mean flow achieved experimentally is compared with theoretical and numerical results. Experimentally we find a non-axisymmetric instability with low azimuthal wavenumber that has inward phase velocity of decreasing magnitude with decreasing radius and small negative wave angle. The data taken from visualizations of the instability waves within the Bödewadt layer suggest a critical Reynolds number $R_d = r^*(\Omega_d^*/\nu^*)^{1/2}$ of 47–56 over a decade range of Ekman numbers.

1 Introduction

Here we study the stability of a laminar mean flow established on the stator of a rotor-stator system. We are interested in the wide-gap limit, such that there are separate boundary layers on both the stator and rotor, with the boundary layer on the stator being closely related to the Bödewadt similarity solution, which is relevant to the single infinite-disk problem. Although the mean flow established in rotor-stator systems is quite well researched, the stability of that flow is less so. There is a greater wealth of research on the related problems of rotating single-disk boundary-layer flows, particularly the von Kármán boundary layer (which forms at a rotating disk when there is stationary fluid sufficiently far above [1]). A characteristic of this flow is inviscid crossflow instability. In the von Kármán boundary layer the crossflow vortices are fixed in the rotating frame of the disk and are the result of interfering wave patterns originating from randomly positioned roughnesses on the surface of the disk. There are travelling waves as well and some of these are predicted to be more unstable. The stationary crossflow vortices, which are the zero-frequency subset of the so-called type-1 mode (a branch of the dispersion relation that is unstable in the inviscid limit), are usually observed in experiments. However, a second mode has been observed [2,3]. These so-called type-2 vortices are a branch of the dispersion relation that is stable in the inviscid limit in the von Kármán boundary layer. The similarities between the single-disk laminar von Kármán and the related Ekman

boundary layer are well established; both flows are susceptible to type-1 and type-2 instabilities. Experimentally, an Ekman layer can be established by modifying the von Kármán flow with the introduction of a geostrophic velocity in the main body of the fluid. In addition to the von Kármán and Ekman boundary-layer flows, Bödewadt [4] studied the steady flow produced over an infinite stationary plane in fluid rotating with uniform angular velocity at an infinite distance from the plane; a problem that (as the von Kármán and Ekman boundary layers) has an exact similarity solution of the Navier–Stokes equations. For this flow there is an equilibrium of centrifugal and radial pressure-gradient forces far from the plane but the centrifugal forces are reduced within the boundary layer causing a radial flow that is predominantly inwards and a consequent upwards axial flow. Linear stability theory predicts that the Bödewadt layer is convectively unstable to both type-1 and type-2 modes.

The Bödewadt similarity solution has one length scale (the boundary-layer thickness $l_f^* = (\nu^*/\Omega_f^*)^{1/2}$) and the non-dimensional control parameter is the local Reynolds number $R_f = r^*(\Omega_f^*/\nu^*)^{1/2}$ (asterisks denote dimensional quantities, r^* is the radial position, Ω_f^* is the free-stream rotation rate and ν^* is the kinematic viscosity). However, for the experimental configuration, consisting of two finite concentric disks of radius R^*, where one rotates (in order to induce fluid rotation) at Ω_d^* and one is stationary, the disk spacing h^* is relevant. Thus, two non-dimensional groups can be formed: typically, the aspect ratio h^*/R^* and the Ekman number $E = \nu^*/(h^{*2}\Omega_d^*)$ (i.e. the ratio of the disk spacing to the boundary-layer length scale $l_d^* = (\nu^*/\Omega_d^*)^{1/2}$, which is essentially an inverse Reynolds number). In this study the aspect ratio takes one fixed value that is sufficiently large for the flow between the two disks to consist of two separate boundary layers for the range of Ekman numbers considered. We also find that the local Reynolds number that varies linearly with the radius $R_d = r^*(\Omega_d^*/\nu^*)^{1/2}$ is still useful.

2 Experimental Description

The experiments described here were performed at the Mechanics Department of KTH, Stockholm. The apparatus consists of two glass disks of diameter $2R^* = 300$ mm that can be independently rotated and that have variable spacing. The disks (labelled A in figure 1) are mounted centrally in a cylindrical Plexiglas water tank (B) of diameter 450 mm. A cylindrical shroud (C) is attached to the edge of the lower disk and there is approximately 1 mm axial clearance between the shroud and the upper disk. For better visualizations of the flow from above the upper surface of the lower disk is coated with a (removable) black covering. The visible disk diameter from above is 260 mm.

The spacing between the disk is fixed at $h^* = 85$ mm, thus the aspect ratio is $h^*/R^* = 0.567$. The out-of-flatness of the lower and upper disks while rotating is less than ± 30 μm and ± 50 μm, respectively. For the Bödewadt flow

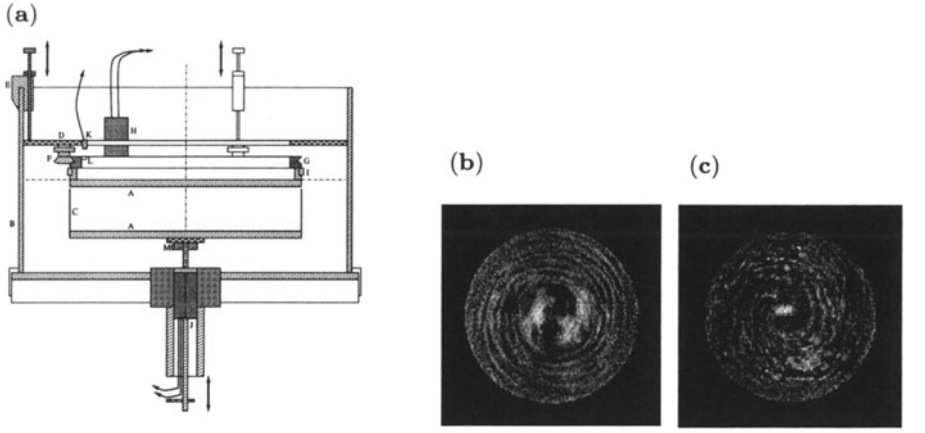

Fig. 1. (**a**) Sketch of the set-up. (**b**) Instabilities within the Bödewadt layer, $R_{do} \approx 146$. (**c**) Turbulence developing, $R_{do} \approx 197$. Anticlockwise rotation. From above

the upper disk is held stationary while the lower disk rotates at Ω_d^*, which implies that the shroud also rotates at Ω_d^*. The fluid is de-aerated water, which fills the tank to a level just below the drive band. The temperature of the water was monitored and found to be $22 \pm 1\,^{\circ}\mathrm{C}$. Throughout the kinematic viscosity of the water will be taken as $1 \times 10^{-6}\ \mathrm{m^2 s^{-1}}$.

We seeded the water with anisotropic reflective flakes (Iriodin) for visualization. Lighting from above gave the clearest images of the flow patterns and formation of vortices that appear as alternate light and dark bands. All images were taken from vertically above. Images from video recordings have been processed using NIH Image software (Internet address: http://rsb.info.-nih.gov/NIH-IMAGE) to obtain qualitative and quantitative information. Particle image velocimetry (PIV) was used to measure two components of the velocity: azimuthal and radial. The same reflective flakes as used for the flow visualization were used as the seeding for the PIV measurements.

3 Experimental Results

Figures 2 (**a**,**b**) show the experimentally measured azimuthal and radial profiles (z is taken positively downwards from the upper stationary disk) for a range of radial positions for $\Omega_d^* \approx 0.348\ \mathrm{rads^{-1}}$ (a speed at which the flow is stable and laminar over almost the full extent of the stationary disk). Clearly the boundary-layer flow is of Batchelor-type but there is radial variation of the angular velocity of the fluid in the core Ω_f^*. Here, therefore, the non-dimensionalization of the experimentally measured velocities is made using the known rotation rate Ω_d^*. The lines plotted for comparison with the experimental data are the Bödewadt similarity solution with various scalings. The variation in the core rotation, caused by the influence of the rotating sidewall, is compared with the numerical data of Dijkstra & van Heijst [5] (taken from their figure 8) in figure 3. They consider the flow between two finite disks with one disk rotating with a cylindrical shroud attached. They solve the

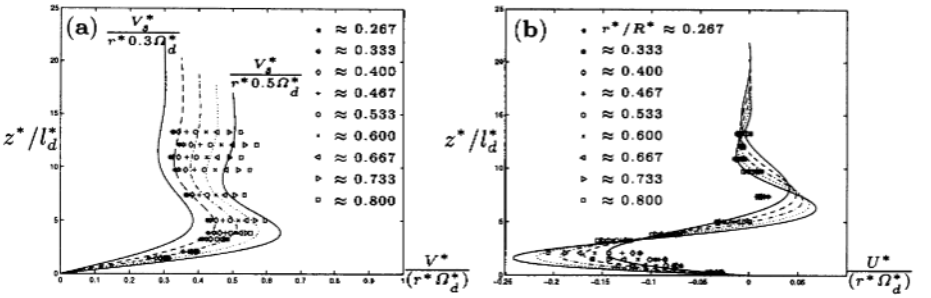

Fig. 2. Experimental velocity profiles for $\Omega_d^* \approx 0.348$ rads^{-1} ($E^{-1} \approx 2517$) compared with scaled similarity solutions (subscript s): (**a**) azimuthal; (**b**) radial profiles

full stationary Navier–Stokes equations using a finite-difference technique. The agreement between our experimental results and this solution is good despite the differences in the measurement location, aspect ratio and Ekman number. As expected the core rotation increases as the rotating shroud is approached. It is possible to achieve a laminar mean flow that closely ap-

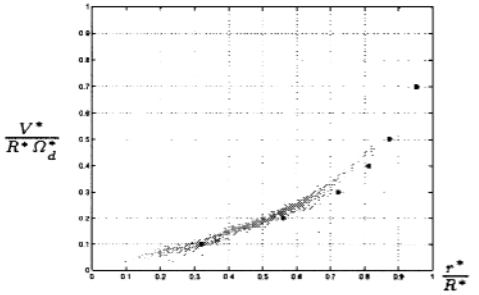

Fig. 3. Numerics for swirl velocity at $z^*/h^* = 0.5$, $h^*/R^* = 0.07$ and $E^{-1} = 1000$ compared with experiments at $z^*/h^* \approx 0.29$, $h^*/R^* \approx 0.57$ and $E^{-1} \approx 2517$ (·)

proximates the Bödewadt layer. Increasing the rotation rate will, however, lead to an increasing region of turbulence, as shown below.

Figure 4 shows a series of images from the PIV camera, in each image the upper disk is stationary but the rotation rate of the lower disk increases through (**a**)–(**i**), thus showing the progression from a stable laminar to a turbulent Bödewadt layer. In (**a**) there are no visible instability waves; in (**b**) waves appear at the outer radius of the disk and propagate inwards into less unstable regions; through images (**c**) to (**g**) these waves progressively reach smaller and smaller radii and become increasingly disordered; in (**h**) and (**i**) the wave structure is lost and the entire boundary layer becomes turbulent. Where the instability waves are visible, the radial wavenumber is approximately constant at 0.55. Table 1 summarizes data taken from a variety of images. The radial location at which the instability waves are no longer visible is $47 < R_{dc} < 56$. The trend is towards the lower end of

Table 1. Data taken from a variety of images. The last two columns (r_c^* and R_{dc}) represent the dimensional and non-dimensional inner radial location, respectively, at which the instability waves are no longer visible in the images

Ω_d^* (rads^{-1})	$E \times 10^5$	R_{do}	r_c^* (mm)	R_{dc}
0.442	31.3	86	85	56
0.685	20.2	108	67	55
0.827	16.7	118	62	56
0.844	16.4	119	61	56
1.265	10.9	146	45	51
1.290	10.7	148	44	50
1.431	9.67	156	41	49
1.852	7.47	177	35	48
1.887	7.33	179	37	51
2.291	7.23	197	33	50
2.332	5.94	199	31	47
2.728	5.07	215	29	48

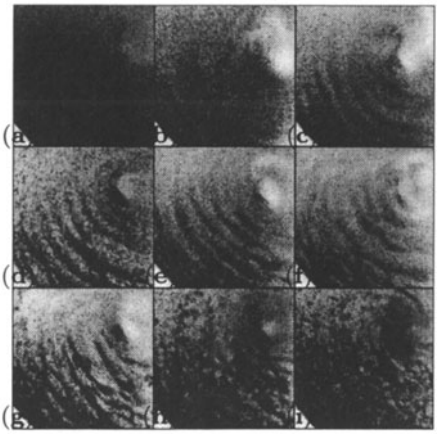

Fig. 4. The Bödewadt layer. (**a**) $\Omega_d^* \approx 0.348$ rads^{-1}; (**b**) $\Omega_d^* \approx 0.685$ rads^{-1}; (**c**) $\Omega_d^* \approx 0.827$ rads^{-1}; (**d**) $\Omega_d^* \approx 1.29$ rads^{-1}; (**e**) $\Omega_d^* \approx 1.43$ rads^{-1}; (**f**) $\Omega_d^* \approx 1.85$ rads^{-1}; (**g**) $\Omega_d^* \approx 2.33$ rads^{-1}; (**h**) $\Omega_d^* \approx 3.64$ rads^{-1}; (**i**) $\Omega_d^* \approx 6.43$ rads^{-1}

this range with increasing rotation rate. This is to be expected because with increasing rotation rate there is an increased outer region of unstable flow in which disturbances can grow to larger amplitudes that can then propagate farther inwards (into less unstable regions) before decaying to such an extent that they are no longer visible. Thus, in this sense, these R_{dc} are lower-bound estimates of the critical Reynolds number for stability because the disturbances may still be visible at Reynolds numbers where they are in fact decaying. However, visualization techniques are inherently insensitive to low-amplitude disturbances and it may be that we lose sight of the disturbance waves before they reach the marginal-stability location. More quantitative measurement techniques would be required to resolve this issue. Note also that some of the variation in R_{dc} may be attributable to variation in local core rotation rate with physical radial location r_c^*.

4 Discussion and Conclusions

Unlike our experiments, in spin-down experiments, such as [6], the boundary layer on the cylindrical wall (which is brought to rest at the initiation of the transient Bödewadt-layer formation) is inherently unstable because the core fluid away from the concave surface is rotating faster, thus producing conditions for centrifugal instability. This is also true for steady experiments designed in such a way that the cylindrical wall is always stationary, and results in Taylor–Görtler vortices convecting within the cylindrical-wall boundary layer towards the end disks possibly convecting into the Bödewadt layer.

Moreover, an impulsive change in rotation rate of the cylinder induces nonlinear inertial oscillations in the core, which may excite the boundary layer. Thus, it was thought that our experimental design allowed for better study of the stability of the Bödewadt layer itself. So far numerical simulations of these flows have been constrained to be axisymmetric and, therefore, only axisymmetric waves have been observed. Further comparison with experimental results and with stability analysis is given in [7].

In the flow above the stationary disk of an enclosed widely-spaced rotor-stator system we find that the azimuthal and radial velocity profiles through the stator boundary layer in the laminar regime have radial variation due to variation in the core azimuthal rotation rate, which increases towards the rotating shroud. The observed radial variation in core azimuthal rotation agrees closely with numerical findings [5] for a similar configuration. The measured local radial and azimuthal velocity profiles compare well with suitably scaled Bödewadt similarity solutions. The experiments show that the boundary layer established on the stator is unstable and that this instability manifests itself as nearly circular waves ($|n| \approx 4$). The wave angle is approximately $-3°$ to $-6°$. The data taken from visualizations of the instability waves within the Bödewadt layer suggests a critical Reynolds number $R_d = r^*(\Omega_d^*/\nu^*)^{1/2}$ of 47–56 over a decade range in Ekman numbers (5.07×10^5 to 58.9×10^5). There is inflow from the edges of the disk and the waves move radially inwards and encounter a stable region at the centre, where fluctuations are suppressed. All the flow visualizations show a region of relative order at the centre; either this region is free from waves or, in the high-Reynolds-number cases, the turbulence in this region loses its coherence (see figure 4). The dominant frequency of the instability has been extracted from images of the flow and is seen to decrease with decreasing radius, having a value of $|\omega^*/\Omega^*| \approx 2$ at $R_d \approx 50$. The radial wavenumber is almost constant (at $0.55/l_d^*$), irrespective of the value of E, over the unstable region. Thus, the radial phase speed decreases in magnitude in the inward direction.

References

1. Kármán, Th. von (1921) Über laminare und turbulente Reibung. Z. Angew. Math. Mech. **1**, 233–252
2. Fedorov, B. I., Plavnik, G. Z., Prokhorov, I. V. & Zhukhovitskii, L. G. (1976) Transitional flow conditions on a rotating disk. J. Engng Phys. **31**, 1448–1453
3. Lingwood, R. J. (1996) An experimental study of absolute instability of the rotating-disk boundary-layer flow. J. Fluid Mech. **314**, 373–405
4. Bödewadt, U. T. (1940) Die Drehströmung über festem Grund. Z. Angew. Math. Mech. **20**, 241–253
5. Dijkstra, D. & Heijst, G. J. F. van (1983) The flow between two finite rotating disks enclosed by a cylinder. J. Fluid Mech. **128**, 123–154
6. Savaş, Ö. (1987) Stability of the Bödewadt flow. J. Fluid Mech. **183**, 77–94
7. Lingwood, R. J. & Alfredsson, P. H. (1999) Experiments on the Bödewadt layer. In preparation.